Received: 24 March 2019 | Revised: 12 July 2019 | Accepted: 12 August 2019

DOI: 10.1111/ejn.14553

RESEARCH REPORT

EJN European Journal of Neuroscience FENS WILEY

Axonal projection-specific differences in somatodendritic α2 autoreceptor function in locus coeruleus neurons

Tobias A. Wagner-Altendorf[1,2] | **Beatrice Fischer**[1] | **Jochen Roeper**[1]

[1]Institute of Neurophysiology, Neuroscience Center, Goethe-University Frankfurt, Frankfurt, Germany

[2]Department of Neurology, University Hospital Schleswig-Holstein, Lübeck, Germany

Correspondence
Jochen Roeper, Institute of Neurophysiology, Neuroscience Center, Goethe-University Frankfurt, Theodor-Stern-Kai 7, Frankfurt 60590, Germany.
Email: roeper@em.uni-franfurt.de

Funding information
Deutsche Forschungsgemeinschaft, Grant/Award Number: CRC 1080; Gutenberg Forschungskolleg

The peer review history for this article is available at https://publons.com/publon/10.1111/EJN.14553

Abstract

The locus coeruleus (LC) contains the majority of central noradrenergic neurons sending wide projections throughout the entire CNS. The LC is considered to be essential for multiple key brain functions including arousal, attention and adaptive stress responses as well as higher cognitive functions and memory. Electrophysiological studies of LC neurons have identified several characteristic functional features such as low-frequency pacemaker activity with broad action potentials, transient high-frequency burst discharges in response to salient stimuli and an apparently homogeneous inhibition of firing by activation of somatodendritic α2 autoreceptors (α2AR). While stress-mediated plasticity of the α2AR response has been described, it is currently unclear whether different LC neurons projecting to distinct axonal targets display differences in α2AR function. Using fluorescent beads-mediated retrograde tracing in adult C57Bl6/N mice, we compared the anatomical distributions and functional in vitro properties of identified LC neurons projecting either to medial prefrontal cortex, hippocampus or cerebellum. The functional in vitro analysis of LC neurons confirmed their mostly uniform functional properties regarding action potential generation and pacemaker firing. However, we identified significant differences in tonic and evoked α2AR-mediated responses. While hippocampal-projecting LC neurons were partially inhibited by endogenous levels of norepinephrine and almost completely silenced by application of saturating concentrations of the α2 agonist clonidine, prefrontal-projecting LC neurons were not affected by endogenous levels of norepinephrine and only partially inhibited by saturating concentrations of clonidine. Thus, we identified a limited α2AR control of electrical activity for prefrontal-projecting LC neurons indicative of functional heterogeneity in the LC-noradrenergic system.

KEYWORDS
alpha receptor, hippocampus, noradrenaline, norepinephrine, prefrontal cortex

Abbreviations: α2AR, α2 adrenergic autoreceptor; ACSF, artificial cerebrospinal fluid; AHP, afterhyperpolarization; AP, action potential; Cb, cerebellum; CNS, central nervous system; DA, dopamine; DAMGO, D-Ala^2,N-Me-Phe^4,Gly^5-ol-enkephalin; dHC, dorsal hippocampus; DMSO, dimethylsulphoxide; GABA, c-aminobutyric acid; GIRK, G protein-coupled inwardly-rectifying potassium channel; LC, locus coeruleus; mPFC, medial prefrontal cortex; NA, noradrenergic; NE, norepinephrine; PBS, phosphate-buffered saline; TH, tyrosine hydroxylase; vHC, ventral hippocampus; VTA, ventral tegmental area.

Edited by Michel Barrot.

1 | INTRODUCTION

The pontine nucleus locus coeruleus (LC) contains the majority—about 10,000–15,000 neurons on each side in humans and 1,500 in rodents—of central noradrenergic neurons that project to a wide variety of targets including cerebellum, prefrontal cortex and hippocampus (Berridge & Waterhouse, 2003; Moore & Bloom, 1979; Swanson, 1976). In line with their broad projections, LC neurons have been implicated in a wide variety of brain functions including arousal, attention, adaptive stress responses, salience and reward processing as well as higher cognition and memory (Aston-Jones & Cohen, 2005; Berridge & Waterhouse, 2003).

Locus coeruleus dysfunction is strongly correlated with several neuropsychiatric disorders including anxiety, depression and post-traumatic stress disorder, while extensive neurodegeneration affects LC neurons both in Parkinson disease and Morbus Alzheimer (Benarroch, 2009).

The locus coeruleus has been generally assumed to operate in a relatively homogenous fashion by broadcasting global tonic and phasic signals via its extensive projections to multiple targets and thereby controlling general brain states (Berridge & Waterhouse, 2003; Loughlin, Foote, & Fallon, 1982). However, more recently studies have revealed an unexpected molecular heterogeneity of LC neurons, which appeared to be associated with distinct axonal projections (Robertson, Plummer, De Marchena, & Jensen, 2013). There is evidence that the LC—similar to the dopaminergic midbrain—contains a heterogeneous set of neurons whose properties vary according to differing terminal fields and that this heterogeneity might provide the functional specialization of monoaminergic systems underlying executive functioning and motivated behaviours (Chandler, Waterhouse, & Gao, 2014; Foote & Berridge, 2018).

On a functional level, there is also renewed interest in projection-specific functions of LC subpopulations given that they have been identified also as major but unexpected sources of dopamine release in structures like the hippocampus, thereby subserving important functions in episodic memory (Kempadoo, Mosharov, Choi, Sulzer, & Kandel, 2016; Takeuchi et al., 2016; Wagatsuma et al., 2018).

In contrast, in other LC projections including those to prefrontal cortex (Deal et al., 2018) and to some thalamic nuclei (Rodenkirch, Liu, Schriver, & Wang, 2019) conventional norepinephrine (NE) release by LC terminals appears to be the dominant mode of action.

In addition to these target-specific differences in differential axonal neurotransmitter release of LC subpopulations, activity control in the somatodendritic area is also more complex than previously suggested. In contrast to LC neuronal activity as an assumed *en masse* population signal, a recent study by Totah and colleagues found surprisingly sparse synchronous LC unit activity, and the cross-correlograms of LC unit pairs provided evidence for complex interaction across multiple time scales (Totah, Neves, Panzeri, Logothetis, & Eschenko, 2018).

Also, Hirschberg and colleagues elegantly demonstrated that spinal- and prefrontal-projecting LC neurons act as antagonistic modules in nociception (Hirschberg, Li, Randall, Kremer, & Pickering, 2017). Apart from being engaged in different neural circuits, they suggested that somatodendritic α2 adrenergic autoreceptor (α2AR)-mediated lateral inhibition—already described by Aghajanian, Cedarbaum, and Wang (1977) using post-stimulatory inhibition as a readout—might contribute to the reciprocal regulation of activity between a "*restorative*" spinal LC module and an "*alarmist*" prefrontal LC module. This raises the question whether another level of functional diversity for LC neurons—similar as previously identified for dopamine midbrain neurons (Lammel et al., 2008)—does also exists at the level of α2AR control and if so whether it is associated with distinct axonal projections.

Previous electrophysiological in vivo and in vitro studies of LC neurons have identified a number of uniform functional features such as broad action potentials, low-frequency pacemaker activity and transient high-frequency burst discharge in response to salient stimuli. In addition, an apparently homogeneous inhibition of firing by somatodendritic α2AR via GIRK channel activation is also a core feature of LC neurons (Arima, Kubo, Ishibashi, & Akaike, 1998; Aston-Jones, Rajkowski, & Cohen, 1999; Nörenberg, Schöffel, Szabo, & Starke, 1997; Williams, Bobker, & Harris, 1991; Williams, North, Shefner, Nishi, & Egan, 1984).

While stress-mediated plasticity of the α2AR-response in LC neurons has been described (Jedema et al., 2008), it is currently unknown whether different LC neurons projecting to distinct axonal targets display baseline differences in α2AR function.

For comparison, relevant differences for somatodendritic autoreceptor function have been identified in the dopaminergic (DA) midbrain system. In contrast to other striatal and non-striatal projection areas, prefrontal-projecting DA mouse neurons localized in the ventral tegmental area (VTA) were found to be unique in their absence of functional somatodendritic D2 autoreceptors (Lammel et al., 2008).

In the present study, we combined in vivo fluorescent beads retrograde tracing with in vitro patch-clamp recordings of retrogradely labelled LC neurons in brainstem slices from adult C57Bl6/N mice to compare anatomical distributions and functional in vitro properties of LC neurons with identified axonal projections. Here, we focus on the differences

between LC neurons projecting to medial prefrontal cortex and those projecting to ventral hippocampus.

2 | MATERIAL AND METHODS

2.1 | Animals

In this study, adult male C57Bl6/N mice (Charles-River, GmbH, Germany), aged 12–13 weeks and weighing 24–26 g at the beginning of the experiments, were used. The animals were housed with free access to water and food with standard 12-hr/12-hr light/dark cycle. All animal protocols were performed according to ethical guidelines approved by the Regierungspräsidium Darmstadt, Germany (F 40/29).

2.2 | Retrograde tracing

The stereotactic surgery for retrograde tracing was performed under 1%–2% isoflurane (in 100% O_2, Forene, Abbott, Wiesbaden, Germany) general anaesthesia. Animals received paracetamol perioperatively (one day before until one day after the operation: 200 µl in 800 ml drinking water; bene Arzneimittel GmbH, Munich, Germany). 0.1 µg/g atropine (Braun, Melsungen, Germany) was applied 20 min preoperatively to prevent bronchoconstriction and hypersalivation. Green and/or red Retrobeads (Lumafluor, Naples, USA) were stereotactically (David Kopf Instruments, Tujunga, USA) infused in the right medial prefrontal cortex (prelimbic and medial orbital areas of mPFC) at four sites with two different bregma sites and two different levels of depth (dorso-ventral axis). At each side (lateral: 0.27 mm, bregma: 2.2 mm and 2.3 mm, dorso-ventral: −2.1 mm and −1.6 mm), 50 nl of undiluted beads solution was infused. For all injection sites, the beads were infused at a rate of 50 nl/min using a 10 µl NanoFil Syringe (WPI Instruments, Berlin, Germany) and a MicroSyringe Pump Controller (WPI Instruments, Berlin, Germany). The needle was kept in place for at least 5 min after infusion, before it was slowly retracted, to avoid backflow. We infused 60 nl of beads solution in either dorsal hippocampus (dHC), at bregma: −2.06 mm, lateral: 1.25 mm, ventral: −1.5 mm, or ventral hippocampus (vHC), at bregma: −3.08 mm, lateral: 2.9 mm, ventral: −4,0 mm. We traced cerebellar cortex (Cb) with 50 nl bead solution at: bregma: −6.3 mm, lateral: 1.5 mm, ventral: 0.9 mm. For dHC, vHC and Cb, we adjusted the bregma coordinates (given by the Paxinos Atlas) for the respective target sites for individual mice according to their lambda-bregma distance (bregma-lambda distance (BL) with the factor bregma(surgery) = (bregma(Paxinos) × 4.2/BL) and added 0.25 mm for dHC and vHC or 0.2 mm for Cb, respectively. This empirical adjustment procedure greatly improved selective tracing.

2.3 | Slice preparation for electrophysiology

At 10–19 days (vHC) and 12–38 days (mPFC), respectively, after retrograde tracing, animals were killed and 220-µm-thick coronal slices of the brain stem including the LC were prepared as previously described (Lammel et al., 2008). Briefly, mice were anesthetized by an overdose of ketamine (500 mg/10 ml; Ratiopharm, Ulm, Germany) and dormitor (1 mg/ml, Pfizer GmbH, Berlin, Germany). Heparin (100 µl; 25,000 I.E./5 ml, ratiopharm) was injected intracardially, followed by transcardial perfusion with an ice-cold artificial cerebrospinal fluid solution (perfusion ACSF) containing in mM: 125 NaCl, 2.5 KCl, 25 $NaHCO_3$, 1.25 NaH_2PO_4, 2.5 Glucose, 50 Sucrose, 6.174 $MgCl_2$, 0.1 $CaCl_2$ and 2.96 kynurenic acid (Sigma-Aldrich), bubbled with carbogen gas (95% O_2 and 5% CO_2), for 5–7 min at a flow rate of about 10–15 ml/min. The brains were rapidly removed, and the brainstem was sliced at 220-µm-thick coronal sections using a vibratome (VT1200S, Leica Microsystems, Wetzlar, Germany). The slices were directly transferred to carbogen-bubbled recording ACSF (in mM: 125 NaCl, 2.5 KCl, 25 $NaHCO_3$; 1.25 NaH_2PO_4, 2.5 Glucose, 22.5 Sucrose, 1 $MgCl_2$, and 2 $CaCl_2$) and allowed to recover for at least 1.5 hr at 37°C before in vitro patch-clamp recordings.

2.4 | Whole-cell patch-clamp recording

In order to perform whole-cell patch-clamp recordings, LC-containing brainstem slices were transferred to a heated (37°C) recording chamber and continuously perfused with 2–4 ml/min carbogen-bubbled recording ACSF, including 10 µM of the non-NMDA glutamate receptor antagonist CNQX, 50 µM NMDA glutamate receptor antagonist DL-AP5 and 10 µM $GABA_A$ receptor antagonist SR95531. For probing the endogenous α2 autoreceptor function, 10 µM α2 receptor antagonist yohimbine was added to the recording ACSF. For proving the effect of maximal α2 autoreceptor stimulation, 1 µM of the α2 receptor agonist clonidine was added to the bath solution. For DAMGO application experiments, 10 µM DAMGO was added to the bath (All substances from Tocris Cookson, Ellisville, USA). LC neurons were included in the study, only when they displayed stable spontaneous pacemaker activity with action potential overshoots >10 mV.

Borosilicate glass pipettes (GC150TF-10, Harvard Apparatus, Kent, UK) were pulled (DMZ Universal puller, Zeitz Instruments GmbH, Munich, Germany) with 4–6 MΩ tip resistance. The pipettes were filled with internal solution containing in mM: 140 KCl, 10 HEPES, 0.1 EGTA, 2 $MgCl_2$ and 1 mg/ml Neurobiotin (NB). LC neurons were visualized by infrared differential contrast videomicroscopy using a digital camera (VX55, Photonics, Pittsfield, MA), mounted to an upright microscope (Axioskop 2, FSplus,

Zeiss, Jena, Germany). Recordings in current clamp were collected using the EPC-10 amplifier (HEKA electronics, Lambrecht, Germany) and PatchMaster v.2.43 software (HEKA electronics).

2.5 | Data analysis

The patch-clamp whole-cell recordings were digitized at 20–50 kHz and filtered at 5 kHz. Spontaneous and evoked action potential firing, sub-threshold responses and action potential wave forms were analysed using Fit master (HEKA electronics) and IGOR pro v6.02a fitted with Neuromatic v2.00 (WaveMetrics Inc., Lake Oswego, USA). Maximum frequencies were analysed by identifying the shortest inter-spike interval during evoked firing from a holding potential of −60 mV in response to increasing 1 s depolarizing currents steps in increments of 50 pA. Action potential thresholds (mV) were determined using the 1st derivative of the AP when the slope >50 mV/ms.

2.6 | Histological analysis

The forebrains of the animals used for in vitro patching were fixed in 4% PFA (in 0.1 M phosphate buffer) for 24–48 hr and then transferred into a storing solution containing 10% sucrose, 0.05% NaN_3 in PBS. The forebrain blocks were sectioned coronally at 100 μm to reconstruct prefrontal or hippocampal injection sites, respectively, using a vibrating slide microtome (VT1000S, Leica Microsystems). Sections with injections sites were counterstained with fluorescent nissl stain (NeuroTrace® 530/615 red fluorescent nissl stain, Invitrogen Molecular Probes, Eugene, USA; 1:100) and analysed by fluorescent microscopy.

Brainstem sections (220 μm) containing recorded and neurobiotin(NB)-filled LC neurons were fixed in 2% PFA (in 0.1 M phosphate buffer, pH 7.4) for 1–3 hr and then transferred to a storing solution for a minimum of 24 hr. Sections were processes for DBH, and TH immunohistochemistry and NB were visualized by fluorescent streptavidin (Molecular Probes, Eugene, USA).

For anatomical analysis of LC neurons after retrograde tracing without additional electrophysiology experiments, animals were anesthetized via i.p. application of 100 μl pentobarbital (16 g pentobarbital sodium/100 ml, Eutha® 77, Essex Tierarznei, Munich, Germany). Heparin (100 μl; 25,000 I.E./5 ml, Ratiopharm) was injected intracardially, followed by transcardial perfusion with 4% PFA in PBS (14 ml/minute for 6 min). The brains were removed and post-fixed overnight and then transferred to storing solution. From brainstem blocks, 60-μm sections containing the LC were prepared for DBH and TH immunohistochemistry. For categorizing the dorso-ventral anatomical positions of LC neurons with identified axonal projections (at bregma −5.4 mm), the LC was divided into 5 dorso-ventral zones (1–5) and each labelled LC neurons was classified to one of the 5 zones.

Histological analysis of prefrontal and hippocampal injection sites for anatomical mapping was performed as described above. In case of cerebellar tracing, due to the neighboured localization of cerebellum and LC, the cerebellar injection sites were sectioned and stained together with the brainstem sections containing the LC (see below).

2.7 | Immunohistochemistry

The free-floating 60-μm (for anatomy) or 220-μm (from patch-clamp experiments; slices were not further sectioned for immunostaining) brainstem sections containing LC were first rinsed in PBS, before non-specific binding was blocked by a 1–3 hr pre-incubation in blocking solution (10% horse serum, 0.2% bovine serum albumin, 0.5% Triton X-100, in PBS). This step was followed by overnight incubation in room temperature with appropriate primary antibodies in carrier solution (1% horse serum, 0.2% bovine serum albumin, 0.5% Triton X-100, in PBS). The following primary antibodies were used: Abcam rabbit anti-DBH "ab43868" (1:750; Cambridge, UK) and Millipore mouse anti-TH "MAB318" (1:2,000; Billerica, USA). On the following day, the sections were rinsed 3 times with PBS, followed by overnight incubation in appropriate secondary fluorescence antibodies. We used the following antibodies: Alexa Fluor® 405 goat anti-mouse, Alexa Fluor® 568 goat anti-rabbit, Alexa Fluor® 647 goat anti-mouse, Alexa Fluor® 647 goat anti-rabbit (all 1:750; all Invitrogen Molecular Probes, Eugene, USA) and Streptavidin Alexa Fluor® 568 (1:000; Molecular Probes, Eugene, USA). Autofluorescence signals were quenched by additionally rinsing sections with 1 mM copper sulphate in 0.01 M ammonium acetate (see Zhang et al., 2010). Finally, sections were rinsed additional three times in PBS before being mounted on glass slides and coverslipped with Vectashield™ (H-1400; Vector Laboratories).

2.8 | Morphological analysis

Confocal microscopy: Sections were analysed using a Zeiss LSM 510 confocal laser-scanning microscope. Fluorochromes were excited by Argon laser using appropriate filter settings, where in patch slices the retrobeads were exited at 488 nm (green), the neurobiotin at 568 nm (red), the DBH at 647 nm (displayed in blue) and the TH at 405 nm (displayed in white). Cell counting of retrogradely labelled LC neurons was performed on confocal images.

Injecting sites: Retrobeads injection sites were analysed with fluorescence microscope BX 61 (Olympus, Hamburg, Germany) and documented with Neurolucida® software (v6.0, MFB Bioscience, Magdeburg, Germany).

2.9 | Statistical analysis

Statistical analyses were performed with unpaired *t* tests or paired *t* tests (for pre–post-clonidine application experiments) and, as indicated, with ANOVA, using Graphpad Prism v5.0c (Graphpad software Inc., La Jolla, USA). The level of significance was set at $p < .05$ (*) and $p < .01$ (**), respectively. Data are presented as mean ± *SEM*.

3 | RESULTS

We defined the anatomical positions of $n = 2{,}013$ retrogradely labelled DBH-(and TH-)immuno-positive LC neurons projecting to either mPFC, vHC, dHC or cerebellum ($N = 16$ mice). In addition, we compared electrophysiological properties and probed somatodendritic α2 autoreceptor functions of $n = 84$ DBH-(and TH-)immuno-positive LC neurons projecting either to mPFC or vHC ($N = 33$ mice).

3.1 | Similar anatomical distribution of LC neurons projecting to mPFC compared with dorsal or ventral hippocampus

In mPFC-traced animals ($N = 4$), we detected $n = 381$ (ca. 95 per animal) retrogradely labelled, that is prefrontal-projecting, DBH-(and TH-)immuno-positive neurons analysing (per animal) 8–11 serial 60-µm sections containing the LC. These LC-mPFC neurons were almost exclusively located in the dorsal half the ipsilateral LC (Figure 1a–c). This anatomical distribution pattern was found across the entire caudo-rostral extent of the LC. Only about 1% of the labelled LC-mPFC neurons ($n = 4/381$) were found within the contralateral LC.

In vHC-traced animals ($N = 3$), we detected $n = 698$ (ca. 233 per animal) retrogradely labelled, ventral hippocampus-projecting DBH-(and TH-)immuno-positive neurons within (per animal) 11–12 serial 60-µm sections containing the LC. The LC-vHC neurons showed a very similar anatomical distribution compared with those of LC-mPFC neurons, that is being clustered in the dorsal half of the LC (Figure 1d–f). In contrast to LC-mPFC neurons, LC-vHC neurons were found to a larger percentage (ca. 10%; $n = 77/698$) on the contralateral side indicative of crossed axonal projections.

We had very similar results for LC neurons projecting to the dHC ($N = 4$ animals), where $n = 633$ (ca. 158 per animal) retrogradely labelled DBH-(and TH-)immuno-positive neurons were identified within (per animal) 7–9 serial 60-µm sections containing the LC (Figure S1a–c). Similar to ventral hippocampal projection, about 15% of the labelled LC-dHC neurons were found to be localized on the contralateral side ($n = 93/633$).

In contrast to these three forebrain projections, DBH-(and TH-)immuno-positive neurons projecting to the cerebellar cortex ($n = 298$ in $N = 3$ animals, ca. 99 per animal; 10–11 serial 60-µm sections) displayed a uniform dorso-ventral distribution across the LC (Figure S1d–f). In addition, about a third of these coeruleo-cerebellar neurons possessed midline-crossing projections (ca. 36%; $n = 107/298$).

Given that we found ~230 retrogradely labelled LC NA neurons per animal after injection of 60 nl retrobeads into the vHC and ~95 retrogradely labelled LC NA neurons per animal after a total injection of 200 nl retrobeads into the mPFC, the LC-vHC projection appears to be fivefold to 10-fold stronger than the LC-mPFC projection.

We also compared the number and distributions of beads-labelled TH-positive neurons in the midbrain (i.e. dopaminergic (DA) neurons). While a substantial number of mPFC-projecting DA neurons were found in the posterior medial VTA—as previously described (Lammel et al., 2008)—we detected only very few ($n < 10$) DA VTA neurons projecting to ventral or dorsal hippocampus and none projecting to cerebellum in all animals (data not shown).

3.2 | Parallel projections from LC neurons to prefrontal cortex and hippocampus

While our tracing data indicated that LC neurons projecting to mPFC and dorsal and ventral hippocampus intermingled in

FIGURE 1 Dorsal clustering of retrogradely identified, independent projections of noradrenergic (NA) locus coeruleus (LC) neurons to medial prefrontal cortex and ventral hippocampus. (a, d) Injection sites for retrograde tracing. Left panels: Corresponding coronal sections taken from Franklin and Paxinos (2007). Right panels: 100-µm coronal sections showing fluorescent bead deposits, red nissl (568 nm) counterstained, of medial prefrontal cortex (mPFC; bregma +2.20 mm; a), and ventral hippocampus (vHC; bregma −3.08 mm; d). Scale bars = 1 mm. (b, e) Representative confocal images of tyrosin hydroxylase (TH-, blue staining) and dopamine-β-hydroxylase (DBH-, red staining) positive LC neurons labelled with green retrobeads in mPFC-traced (b) and vHC-traced (e) animals. Scale bars = 20 µm. (c, f) Schematic representation of topographical distributions of retrogradely labelled mPFC- and vHC-projecting TH^+/DBH^+ LC neurons. Note that both groups are clustered in the dorsal LC. One red symbol represents 2 labelled TH^+/DBH^+ LC neurons in the central portion of the LC (between bregma −5.3 and −5.5 mm). (g) Injection sites for double retrograde tracings, using green fluorescently labelled latex beads for mPFC (red nissl counterstained, top panel) and red fluorescently labelled latex beads for vHC (green nissl counterstained, bottom panel). (h) Left: Immunostaining of the LC ipsilateral to tracing sites mPFC (green beads) and vHC (red beads), stained for DBH (blue). LC-mPFC and LC-vHC neurons cluster in the dorsal half of the LC with little overlap, in a "salt-and-pepper" distribution pattern. Scale bar = 50 µm. Right, top: Individual LC-mPFC and LC-vHC neurons are next to each other. Right, bottom: Example of a double labelled LC neuron. Scale bars = 10 µm. (i) Average numbers of mPFC- ($N = 4$ animals), vHC- ($N = 3$ animals) and double-projecting (mPFC+vHC; $N = 2$ animals) TH^+/DBH^+ LC neurons. Note that less than 1% of the cells are double labelled (Kruskal–Wallis one-way ANOVA: $p = .03$). [Colour figure can be viewed at wileyonlinelibrary.com]

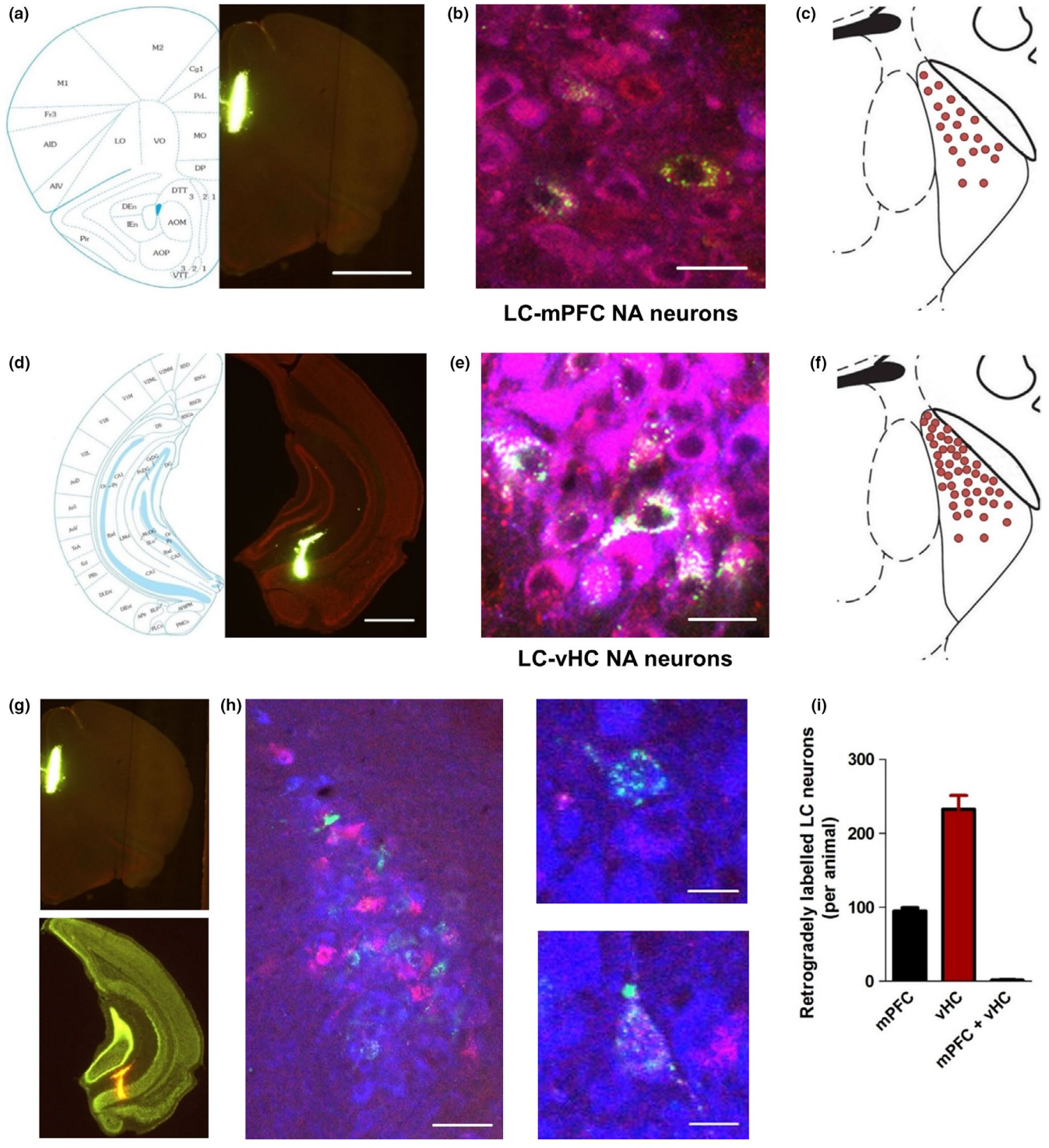

the dorsal part of the LC in salt-and-pepper fashion, they did not address whether individual LC neurons might project to both areas by axonal branching. Thus, we carried out double retrograde tracing in mPFC and vHC using differently coloured beads. Figure 1 g–i shows that LC-mPFC and LC-vHC neurons are often direct neighbours within the dorsal LC, but <1% of LC neurons (n = 3/656; N = 2 animals) displayed double colour-labelling indicative of axonal branches in both mPFC and vHC. These experiments strongly suggest that mPFC- and vHC-projecting LC neurons are best described as anatomically segregated, parallel lines.

3.3 | Distinct afterhyperpolarizations at baseline conditions between mPFC- and vHC-projecting LC neurons

We recorded from two identified LC subgroups in vitro, the coeruleo-prefrontal (i.e. LC-mPFC NA neurons) and the

coeruleo-hippocampal (i.e. LC-vHC NA neurons) populations. The two LC neuronal groups were both investigated under baseline conditions as well as in the presence of the α2AR blocker yohimbine (10 μM) to suppress a potential α2AR tone preserved in in vitro brainstem slices. In addition to spontaneous intrinsic properties, we carried out recordings of LC neurons where we applied 1 μM α2AR agonist clonidine to test for autoreceptor function and 10 μM of the μ-opioid receptor agonist DAMGO to compare for autoreceptor-independent GPCR signalling. All recorded LC neurons were identified by retrograde tracing and visualized by neurobiotin labelling and DBH/TH immunohistochemistry (Figure 2a).

At baseline in vitro conditions, LC-mPFC NA neurons displayed a mean spontaneous frequency of 2.4 ± 0.2 Hz ($n = 16$). In comparison, LC-vHC NA neurons discharged in a very similar mean frequency range of 2.3 ± 0.2 Hz ($n = 19$). Also, analysis of single action potential (AP) parameters showed similar AP widths and maxima for the two groups: for the coeruleo-prefrontal subpopulation, experiments revealed a mean AP width (*at threshold*) of 3.4 ± 0.4 ms ($n = 13$) and a mean AP peak of 31.0 ± 2.0 ms ($n = 16$); for the coeruleo-hippocampal subpopulation, LC neurons possessed a mean AP width of 3.0 ± 0.1 ms ($n = 15$) and a mean AP peak of 32.1 ± 1.4 mV ($n = 17$). In contrast to these very similar electrophysiological properties, our analysis revealed significant differences between amplitudes of afterhyperpolarizations (AHP): LC-mPFC NA neurons had a mean AHP minimum of −63.3 ± 1.2 mV ($n = 16$) with a mean AP threshold of −31.3 ± 1.0 mV ($n = 16$), while LC-vHC NA neurons displayed a significantly more negative mean AHP minimum at −68.0 ± 1.0 mV ($n = 17$; $p = .005$) with mean AP threshold of −34.1 ± 0.9 mV ($n = 17$; $p = .04$; Figure 2b,c).

3.4 | Different sub-threshold electrophysiological properties at baseline between LC-mPFC and LC-vHC NA neurons

Applying step-wise increasing depolarizing currents, we defined firing frequency-current (f-I) relationships for both LC-mPFC and LC-vHC NE neurons, which appeared to be very similar between the two groups (Figure 3a). Also, maximum discharge frequencies—before the onset of depolarization block—did not differ significantly (LC-mPFC: 61.5 ± 7.3 Hz ($n = 14$); LC-vHC: 59.6 ± 5.9 Hz ($n = 13$)).

In contrast, the sub-threshold electrophysiological properties of LC-mPFC and LC-vHC NA neurons were significantly different. In comparison with LC-vHC NA neurons, LC-mPFC NA neurons showed smaller membrane hyperpolarizations induced by injection of negative currents ranging from −25 to −75 pA (Figure 3b; injection of −75 pA: LC-mPFC: −80.2 ± 3.0 mV ($n = 15$); LC-vHC: −89.0 ± 2.3 mV ($n = 19$; $p = .03$). As LC-mPFC NA neurons showed less negative AHPs during spontaneous pacemaker activity as well as smaller membrane hyperpolarizations by negative current injections, we reasoned that these coerulo-prefrontal NA neurons might possess differences in intrinsic excitability or limited α2 autoreceptor function, which is known to activate a hyperpolarizing potassium conductance.

3.5 | α2AR inhibition unmasks faster baseline pacemaking in LC-vHC compared with LC-mPFC NA neurons

We recorded in the presence of 10 μM yohimbine to inhibit the potential contribution of an endogenous NA α2 autoreceptor tone to the different properties of axonal projection identified LC NA neurons described above. Indeed, in yohimbine, LC-vHC NA neurons displayed an about 30% faster firing frequency compared to baseline conditions (2.3 ± 0.2 Hz; $n = 19$ vs. 3.0 ± 0.3 Hz; $n = 13$; $p = .04$). In contrast, pacemaker frequencies of LC-mPFC NA neurons were not different in the presence of 10 μM yohimbine compared with baseline (2.4 ± 0.2 Hz; $n = 16$ vs. 2.2 ± 0.2 Hz; $n = 13$). These data also imply that LC-vHC NA neurons fired significantly faster during α2AR inhibition compared with LC-mPFC NA neurons (Figure 4a, LC-vHC: 3.0 ± 0.3 Hz, $n = 13$; LC-mPFC: 2.3 ± 0.2 Hz, $n = 13$; $p = .03$). These experiments suggested a smaller if not absent control via somatodendritic α2AR in those LC neurons projecting to mPFC under in vitro brain slice conditions.

Additional analysis of action potential AHPs and sub-threshold properties revealed that the identified baseline differences, reported above, were absent in the presence of yohimbine and (Figure 4b, AHPs: LC-mPFC: −59.6 ± 1.1 mV ($n = 13$); LC-vHC: −59.9 ± 1.6 mV ($n = 13$); Figure 4c, under injection of −75pA: LC-mPFC: −80.9 ± 4.4 mV ($n = 13$); LC-vHC: −75.9 ± 4.7 mV ($n = 13$)).

3.6 | α2 autoreceptor activation via clonidine does not silence LC-mPFC NA neurons

To further investigate the observed differences in putative α2AR signalling in LC-mPFC compared to LC-vHC NA neurons, we carried out patch-clamp experiments with direct application of α2AR agonist clonidine. After wash-in of 1 μM clonidine, LC-vHC NA neurons showed a nearly complete silencing (85% reduction) of spontaneous firing (control: 2.7 Hz ± 0.3 Hz; 1 μM clonidine: 0.4 ± 0.2 Hz ($n = 12$)), while LC-mPFC NA neurons were significantly less affected (<50% reduction) by 1 μM clonidine (control: 2.2 Hz ± 0.4 Hz; 1 μM clonidine: 1.4 ± 0.4 Hz ($n = 11$); $p = .01$ for inhibition of firing frequency LC-mPFC vs. LC-vHC). Analysis of the mean membrane potentials before and after clonidine wash-in also revealed a significant hyperpolarization of membrane potential by clonidine in

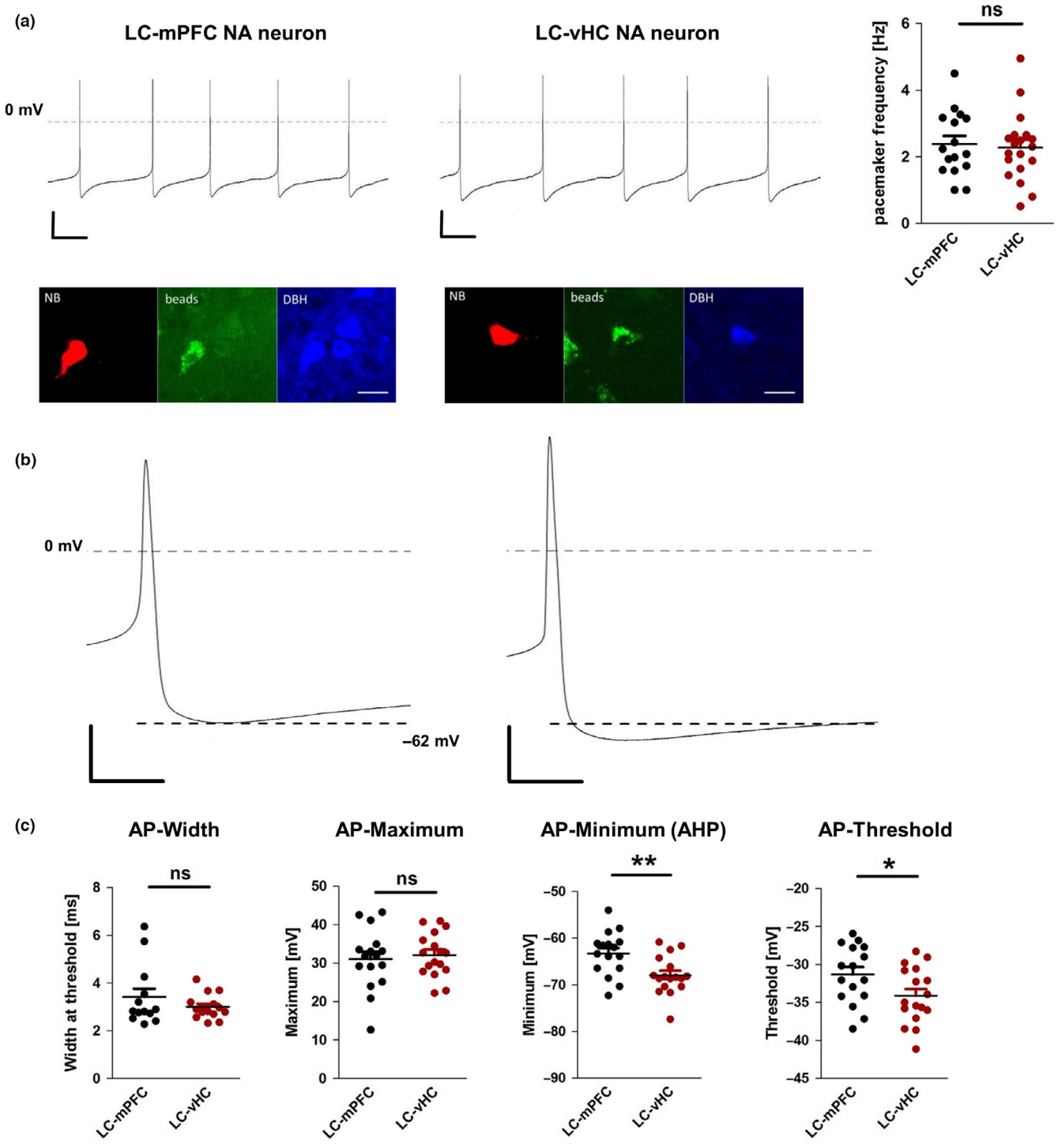

FIGURE 2 LC-mPFC NA neurons possess similar firing frequencies, but smaller AHPs compared to LC-vHC NA neurons. (a) Left and middle upper panel: Current-clamp (whole-cell) recordings of retrogradely identified, representative LC-mPFC and LC-vHC NA neurons. Scale bars = 20 mV, 200 ms. Right upper panel: Mean spontaneous discharge frequencies of identified LC-mPFC (n = 16) and LC-vHC (n = 19) NA neurons. Lower panels: All recorded LC-mPFC and LC-vHC NA neurons were filled with neurobiotin during recording and fixed for post hoc identification. Neurobiotin-streptavidin-568 (red), fluorescent latex beads (green), DBH-antibody (blue). Scale bars = 20 µm. (b) Single action potentials of retrogradely identified, representative LC-mPFC and LC-vHC NA neurons. LC-mPFC NA neurons show significantly depolarized AHP amplitudes compared to LC-vHC NA neurons. Scale bars = 20 mV, 10 ms. (c) Distribution of mean AHP minima, threshold potentials, AP widths and maxima of identified LC-mPFC (n = 13–16) and LC-vHC (n = 15–17) NA neurons. While AP widths and maxima do not differ, AHP minima and threshold potentials are differing significantly between subpopulations (p = .005 and p = .04, respectively, unpaired t test). [Colour figure can be viewed at wileyonlinelibrary.com]

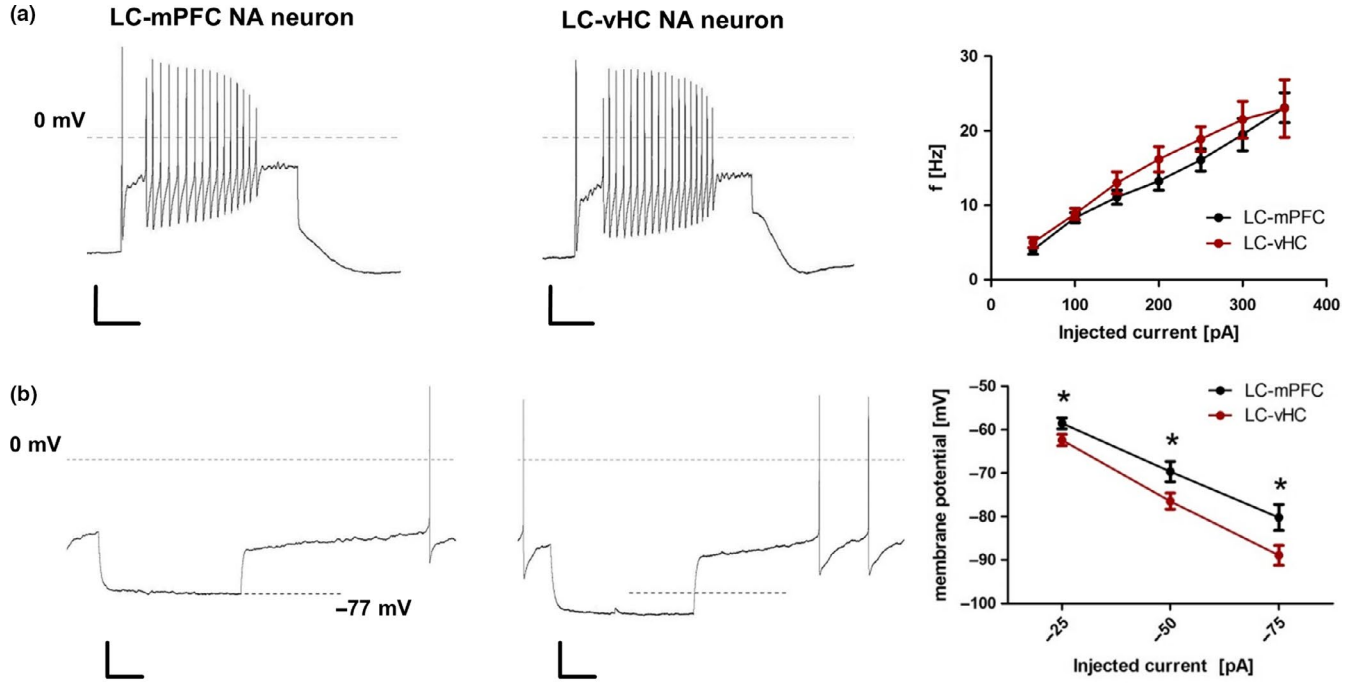

FIGURE 3 LC-mPFC NA neurons show similar super-threshold behaviour (f-I curves), but smaller sub-threshold responses compared to LC-vHC NA neurons. (a) Left and middle panel: Current-clamp (whole-cell) recordings of retrogradely identified, representative LC-mPFC and LC-vHC NA neurons, under injection of depolarizing current. Scale bars = 20 mV, 250 ms. Right panel: Mean frequency–current curves (with *SEM*) of LC-mPFC and LC-vHC NA neurons. (b) Left and middle panel: Current-clamp (whole-cell) recordings of retrogradely identified, representative LC-mPFC and LC-vHC NA neurons, under injection of depolarizing current (−75 pA). Scale bars = 20 mV, 500 ms. Right panel: Mean potential–current curves (with *SEM*.) of LC-mPFC and LC-vHC NA neurons. LC-mPFC NA neurons show a significantly reduced hyperpolarization after injection of −25 pA ($p = .04$), −50 pA ($p = .03$) and −75 pA ($p = .03$) (all unpaired *t*-test) (two-way ANOVA: $p = .0002$). [Colour figure can be viewed at wileyonlinelibrary.com]

LC-vHC NA neurons (control: −40.6 ± 0.9 mV; clonidine: −44.4 ± 1.9 mV ($n = 12$; $p = .02$)) but no hyperpolarization of membrane potential by clonidine in LC-mPFC NA neurons (control: −40.2 ± 1.2 mV; clonidine: −40.0 ± 1.4 mV ($n = 11$)). These additional pharmacological experiments provided independent support for differences in autoreceptor signalling between the two LC subpopulations.

To exclude the possibility that general GPCR signalling was impaired in LC-mPFC NA neurons, for example by the whole-cell configuration, we tested μ-opioid receptor activation with 1 μM DAMGO. Here, both LC-mPFC ($n = 4$) and LC-vHC NA neurons ($n = 6$) displayed a complete silencing of pacemaker frequency that was accompanied on substantial membrane hyperpolarization (Figure 5).

In summary, our data identified functionally distinct LC subpopulations according to their non-overlapping axonal projections that are likely to possess different degrees of control by somatodendritic α2 autoreceptors.

4 | DISCUSSION

The present study we investigated anatomical and in vitro electrophysiological properties of immunohistochemically identified, noradrenergic locus coeruleus neurons with distinct axonal projections. We found that, while displaying similar (but not identical) electrophysiological properties under baseline in vitro conditions, coeruleo-prefrontal (LC-mPFC) and coeruleo-hippocampal (LC-vHC) projecting LC NA neurons differed strongly under pharmacological conditions most consistent with α2 autoreceptor inhibition or activation. In particular and in contrast to hippocampus-projecting LC NA neurons, LC-mPFC NA neurons were not affected by an endogenous norepinephrine tone in the brain slice and only partially inhibited by pharmacological α2 autoreceptor activation. While LC NA neurons have been traditionally regarded as a functionally very homogeneous group (Berridge & Waterhouse, 2003; Williams et al., 1984), Chandler and colleagues already reported that LC-mPFC NA neurons were more excitable compared to LC neurons projecting to other cortical areas (Chandler, Gao, & Waterhouse, 2014). However, this study did not address the issue whether the difference in excitability were mediated by differential autoreceptor tone.

These differences might open the general possibility of hierarchical control via α2 autoreceptor activation among locus coeruleus subpopulations in the sense that activity-dependent NE release from mPFC-projecting LC

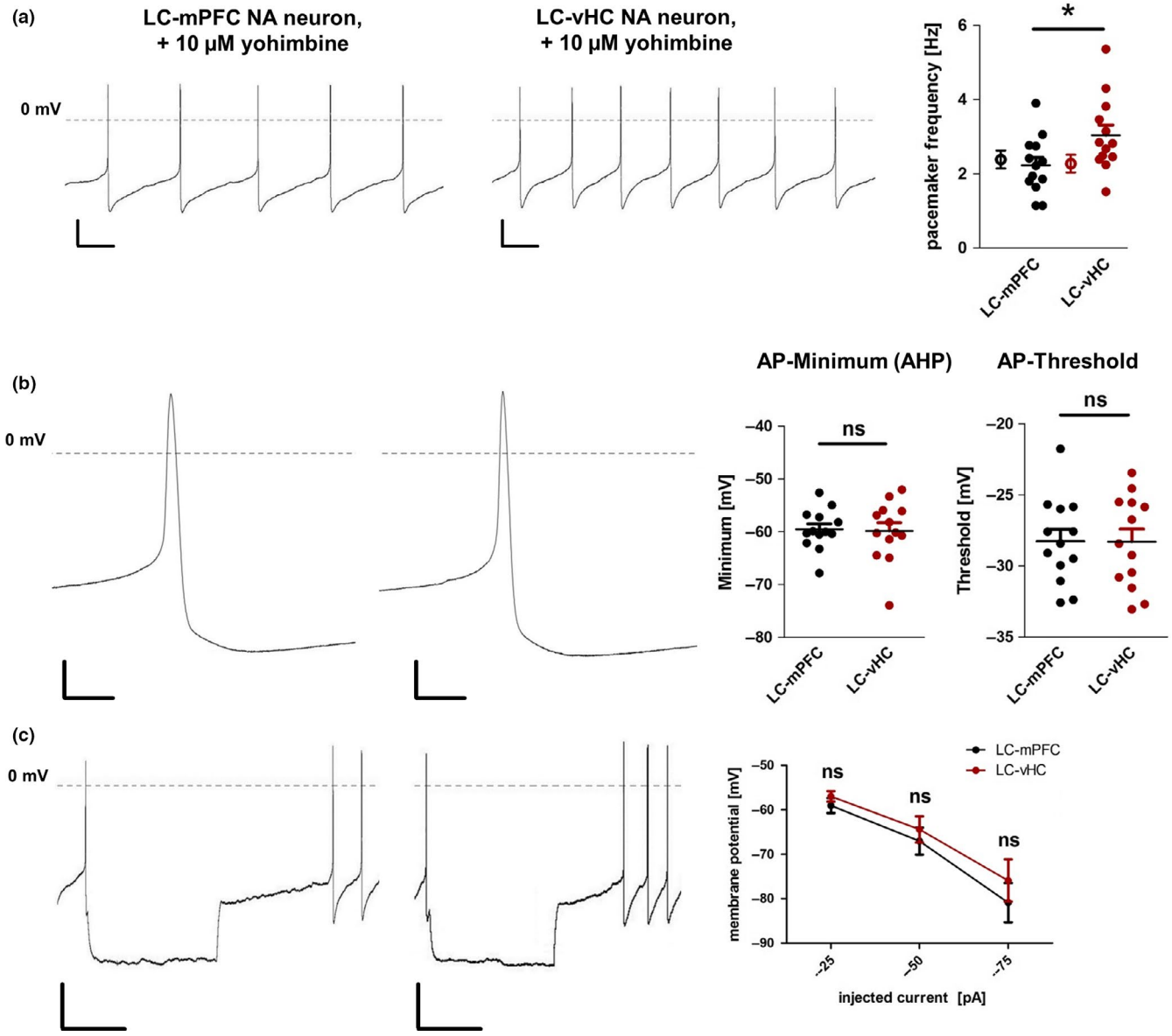

FIGURE 4 α2 autoreceptor inhibition reveals lower sensitivity to endogenous NA tone of LC-mPFC NA neurons compared to LC-vHC NA neurons. (a) Left and middle panel: Current-clamp (whole-cell) recordings of retrogradely identified, representative LC-mPFC and LC-vHC NA neurons, under α2 autoreceptor inhibition with 10 µM yohimbine. Scale bars = 20 mV, 200 ms. Right panel: Mean spontaneous discharge frequencies of LC-mPFC ($n = 13$) and LC-vHC ($n = 13$) NA neurons under α2 inhibition. Single black symbol and single red symbol represent mean firing frequency without α2 inhibition in LC-mPFC and LC-vHC NA neurons, respectively. Under α2 inhibition with yohimbine, LC-vHC NA neurons show significantly faster intrinsic pacemaking than LC-mPFC NA neurons ($p = .03$; unpaired t test), while LC-mPFC NA neurons show no significant alteration of frequency. (b) Left and middle panel: Single action potentials of retrogradely identified, representative LC-mPFC and LC-vHC NA neurons, under α2 autoreceptor inhibition with 10 µM yohimbine. Scale bars = 10 mV, 10 ms. Right panel: Distribution of mean AHP minima and threshold potentials of identified LC-mPFC ($n = 13$) and LC-vHC ($n = 13$) NA neurons. Under α2 autoreceptor inhibition, no significant differences in AHP and threshold potentials between the groups are present. (c) Left and middle panel: Current-clamp (whole-cell) recordings of retrogradely identified, representative LC-mPFC and LC-vHC NA neurons, under injection of depolarizing current (−75 pA) and α2 autoreceptor inhibition with 10 µM yohimbine. Scale bars = 20 mV, 1 s. Right panel: Mean potential–current curves (with SEM) of LC-mPFC and LC-vHC NA neurons. Under α2 autoreceptor inhibition, curves do not differ significantly (two-way ANOVA: $p = .23$). [Colour figure can be viewed at wileyonlinelibrary.com]

neurons might result in α2 autoreceptor activation and in turn inhibition of, for example, hippocampus-projecting LC neurons. Given that our anatomical data demonstrated that cell bodies of mPFC- and HC-projecting LC NA neurons intermingle in the dorsal half of the LC but are segregated from other LC populations like those projecting to cerebellum, this directed local control among two LC populations might be plausible. However, whether a differential α2 autoreceptor tone among mPFC- and vHC-projecting LC NA neurons is present in vivo is currently

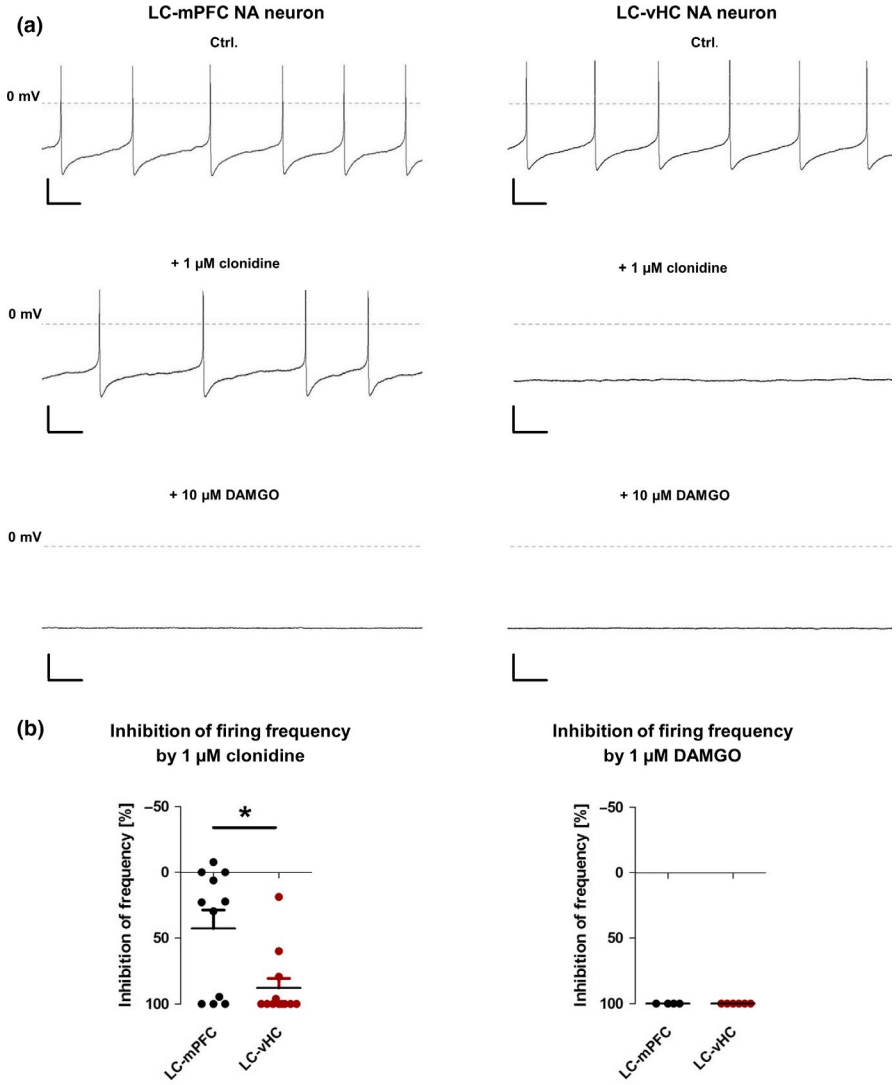

FIGURE 5 LC-mPFC NA neurons show limited α2 autoreceptor function compared to LC-vHC NA neurons. (a) Current-clamp (whole-cell) recordings of retrogradely identified, representative LC-mPFC and LC-vHC NA neurons, before and during wash-in of a saturating concentration (1 µM) of the α2 autoreceptor agonist clonidine (upper and middle panels), and during wash-in of 10 µM opioid receptor agonist DAMGO (lower panels). Scale bars = 20 mV, 200 ms. (b) Distribution of mean inhibitions of firing rate of identified LC-mPFC and LC-vHC NA neurons, before and during wash-in of α2 agonist clonidine (left) and µ-opioid receptor agonist DAMGO (right). LC-mPFC NA neurons ($n = 11$) show a reduced α2-mediated inhibition of firing frequency compared to LC-vHC NA neurons ($n = 12$) (42.6% vs. 87.9%; $p = .01$), while both groups are equally silenced by µ-opioid receptor activation. [Colour figure can be viewed at wileyonlinelibrary.com]

unknown but can now be experimentally addressed in future experiments. This might be of particular interest during brain functions like episodic or working memory where mPFC and HC operate in a functionally coupled network (Eichenbaum, 2017). Also, our anatomical data are in line with previous topographic studies of the rat LC system (Loughlin, Foote, & Bloom, 1986; Loughlin et al., 1982; Mason & Fibiger, 1979) as well as more recent viral genetic tracing studies in mice (Schwarz et al., 2015). Importantly, our double tracing studies with differently coloured fluorescent beads established that LC neurons projecting to mPFC and those projecting to hippocampal targets are essentially non-overlapping parallel lines. This result is in line with recent studies demonstrating molecularly and anatomical heterogeneous LC subpopulations (Chandler et al., 2014). Moreover, if mPFC-projecting LC neurons would be indeed unique among other LC subpopulations targeting different cortical or subcortical areas regarding their limited autoreceptor control, this mechanism might help to support—in addition to circuit mechanisms (Aston-Jones & Waterhouse, 2016)—a low arousal brain state where mPFC function is relatively selectively boosted for, for example safety learning in the context of fear conditioning, while other LC projections to, for example, sensory cortices, hippocampus, amygdala or brainstem targets would dominate in a more stressful/high arousal state with impaired mPFC function (Thiele & Bellgrove, 2018). Recent optogenetic targeting approaches have provided evidence for projection-specific antagonism (fear vs. extinction memory; analgesia vs. aversion/anxiety) among mPFC-projecting and distinct subcortical-projecting LC subpopulations (Hirschberg et al., 2017; Uematsu et al., 2017). This mode of LC function using an array of parallel lines has also recently been reviewed as "polymorphic computation" (Seo & Bruchas, 2017). In this context, our finding of reduced autoreceptor control for mPFC-projecting LC NA neurons would endow this polymorphic computer with an additional level of contrast enhancement between the LC array elements (see Figure 1b, Seo & Bruchas, 2017).

A more direct implication of our findings would be the prediction that in vivo manipulations of α2 autoreceptors in the locus coeruleus would differently affect NE release in mPFC compared with other areas. Indeed, a microdialysis study by Parini, Renoldi, Battaglia, and Invernizzi (2005) reported a 40% reduction in extracellular prefrontal NE compared with a 65% reduction in extracellular hippocampal NE in vivo after infusion of the α2 agonist clonidine (0.6 nmol/0.5 ml) into the LC. In contrast, systemic application of NE-reuptake inhibitor reboxetine led to an identical increase in NE concentrations in hippocampus and prefrontal cortex (HC: +240%, mPFC: +242%) supporting the notion of local signalling differences for the distinct projection within the LC. It should, however, be noted that local infusion of drugs into the LC in vivo does not guarantee selective action on somatodendritic α2 autoreceptors but might need a cell- and projection-selective genetic strategy (e.g. Li et al., 2016).

Finally, our findings do identify but not reveal the underlying mechanism of reduced α2 autoreceptor function in mPFC-projecting LC NA neurons. Given that these neurons generated strong μ-opioid receptor-mediated membrane hyperpolarizations very similar to other LC neurons suggested that they express sufficient GIRK channels (Lüscher & Slesinger, 2010) but might have a lower number of somatodendritically expressed a2AR and/or a reduced coupling of this particular type of GPCR receptor to GIRK channels. While no projection-related differences under baseline conditions have been reported before (but note e.g. that the degree of α2AR-mediated inhibition by intermediate clonidine concentrations varied between 50% and 100%; Jedema et al., 2008), impairments of α2AR coupling in response to chronic cold stress during amphetamine sensitization have been reported (Doucet et al., 2013; Jedema et al., 2008). These studies suggested several mechanisms including altered expression of G-alphaI proteins and regulators of GPCR signalling (RGS7) in LC neurons, but did not demonstrate causality or projection specificity. Given that all our experimental animals received stereotactic surgery for retrograde tracing 2–3 weeks before recording, we cannot rule out that stress effects might have contributed to the reported differences in projection-specific autoreceptor function. In any case, future studies recording projection-defined LC neurons in vivo are needed to define the functional contribution and plasticity of reduced α2AR control in mPFC-projecting LC NA neurons for multiple brain functions as well as for stress- and disease-related brain states.

4.1 | Limitations of the study

Some technical limitations of our study have to be discussed. We used whole-cell patch-clamp recordings to characterize retrogradely identified LC NA neurons. While this provides low-resistance access to the cell, this configuration also perturbs the intracellular milieu by dialysis with the pipette solution. We cannot formally exclude that this might have differentially affected the α2AR-signalling in the two LC subpopulations. However, as firing frequencies in both LC populations were stable over time, we believe this situation is not likely.

Another caveat is that our conclusions are based on pharmacological tools only. While we used prototypical drugs for α2AR manipulations, potential off-target effects cannot be discarded a priori and an independent validation, for example by molecular strategy using knockout animals would have provided additional evidence. Future experiments thus could also utilize UK14304 as a full α2AR agonist to further differentiate α2AR function in projection-specific subtypes of noradrenergic locus coeruleus neurons.

ACKNOWLEDGEMENTS

We thank Annika Parg for her excellent technical support and Sabine Krabbe for teaching TWA to use the Roeper laboratory protocol for in vivo fluorescent bead tracing. Research was supported by funding to JR (CRC1080, DFG and Gutenberg Research College).

CONFLICT OF INTEREST

The authors declare no competing financial interests.

DATA AVAILABILITY STATEMENT

In accordance with the "DFG Guidelines on the Handling of Research Data", we will make all data (digitized electrophysiological recordings (IGOR wave metrics format); confocal images (a.o. TIFF format) available upon request. The data set will be archived for at least 10 years after publication.

AUTHOR CONTRIBUTIONS

TWA carried out retrograde tracing, in vitro electrophysiology, immunocytochemistry, confocal microscopy and data analysis. BK carried out additional retrograde tracing and immunocytochemistry. JR carried out in vitro electrophysiology for the clonidine/DAMGO application experiments. TWA and JR designed the study, analysed data and wrote the manuscript.

ORCID

Jochen Roeper https://orcid.org/0000-0003-2145-8742

REFERENCES

Aghajanian, G. K., Cedarbaum, J. M., & Wang, R. Y. (1977). Evidence for norepinephrine-mediated collateral inhibition of locus coeruleus neurons. *Brain Research*, *136*(3), 570–577.

Arima, J., Kubo, C., Ishibashi, H., & Akaike, N. (1998). α2-Adrenoceptor-mediated potassium currents in acutely dissociated rat locus coeruleus neurones. *The Journal of Physiology*, *508*(1), 57–66.

Aston-Jones, G., & Cohen, J. D. (2005). An integrative theory of locus coeruleus-norepinephrine function: Adaptive gain and optimal performance. *Annual Review of Neuroscience*, *28*, 403–450.

Aston-Jones, G., Rajkowski, J., & Cohen, J. (1999). Role of locus coeruleus in attention and behavioral flexibility. *Biological Psychiatry*, *46*(9), 1309–1320.

Aston-Jones, G., & Waterhouse, B. (2016). Locus coeruleus: From global projection system to adaptive regulation of behavior. *Brain Research*, *1645*, 75–78.

Benarroch, E. E. (2009). The locus ceruleus norepinephrine system Functional organization and potential clinical significance. *Neurology*, *73*(20), 1699–1704.

Berridge, C. W., & Waterhouse, B. D. (2003). The locus coeruleus–noradrenergic system: Modulation of behavioral state and state-dependent cognitive processes. *Brain Research Reviews*, *42*(1), 33–84.

Chandler, D. J., Gao, W. J., & Waterhouse, B. D. (2014). Heterogeneous organization of the locus coeruleus projections to prefrontal and motor cortices. *Proceedings of the National Academy of Sciences of the United States of America*, *111*, 6816–6821.

Chandler, D. J., Waterhouse, B. D., & Gao, W. J. (2014). New perspectives on catecholaminergic regulation of executive circuits: Evidence for independent modulation of prefrontal functions by midbrain dopaminergic and noradrenergic neurons. *Frontiers in Neural Circuits*, *8*, 53.

Deal, A. L., Mikhailova, M. A., Grinevich, V. P., Weiner, J. L., Gainetdinov, R. R., & Budygin, E. A. (2018). In vivo voltammetric evidence that locus coeruleus activation predominantly releases norepinephrine in the infralimbic cortex: Effect of acute ethanol. *Synapse (New York, N. Y.)*, *73*, e22080.

Doucet, E. L., Bobadilla, A. C., Houades, V., Lanteri, C., Godeheu, G., Lanfumey, L., … Tassin, J. P. (2013). Sustained impairment of α2A-adrenergic autoreceptor signaling mediates neurochemical and behavioral sensitization to amphetamine. *Biological Psychiatry*, *74*(2), 90–98.

Eichenbaum, H. (2017). Prefrontal–hippocampal interactions in episodic memory. *Nature Reviews Neuroscience*, *18*(9), 547.

Foote, S. L., & Berridge, C. W. (2018). New developments and future directions in understanding locus coeruleus–Norepinephrine (LC-NE) function. *Brain Research*.

Franklin, K. B. J., & Paxinos, G. (2007). *The mouse brain in stereotactic coordinates* (3rd ed.). Cambridge, MA: Academic Press.

Hirschberg, S., Li, Y., Randall, A., Kremer, E. J., & Pickering, A. E. (2017). Functional dichotomy in spinal-vs prefrontal-projecting locus coeruleus modules splits descending noradrenergic analgesia from ascending aversion and anxiety in rats. *eLife*, *6*, e29808.

Jedema, H. P., Gold, S. J., Gonzalez-Burgos, G., Sved, A. F., Tobe, B. J., Wensel, T. G., & Grace, A. A. (2008). Chronic cold exposure increases RGS7 expression and decreases α2-autoreceptor-mediated inhibition of noradrenergic locus coeruleus neurons. *European Journal of Neuroscience*, *27*(9), 2433–2443.

Kempadoo, K. A., Mosharov, E. V., Choi, S. J., Sulzer, D., & Kandel, E. R. (2016). Dopamine release from the locus coeruleus to the dorsal hippocampus promotes spatial learning and memory. *Proceedings of the National Academy of Sciences*, *113*(51), 14835–14840.

Lammel, S., Hetzel, A., Häckel, O., Jones, I., Liss, B., & Roeper, J. (2008). Unique properties of mesoprefrontal neurons within a dual mesocorticolimbic dopamine system. *Neuron*, *57*(5), 760–773.

Li, Y., Hickey, L., Perrins, R., Werlen, E., Patel, A. A., Hirschberg, S., … Pickering, A. E. (2016). Retrograde optogenetic characterization of the pontospinal module of the locus coeruleus with a canine adenoviral vector. *Brain Research*, *1641*, 274–290.

Loughlin, S. E., Foote, S. L., & Bloom, F. E. (1986). Efferent projections of nucleus locus coeruleus: Topographic organization of cells of origin demonstrated by three-dimensional reconstruction. *Neuroscience*, *18*(2), 291–306.

Loughlin, S. E., Foote, S. L., & Fallon, J. H. (1982). Locus coeruleus projections to cortex: Topography, morphology and collateralization. *Brain Research Bulletin*, *9*(1–6), 287–294.

Lüscher, C., & Slesinger, P. A. (2010). Emerging roles for G protein-gated inwardly rectifying potassium (GIRK) channels in health and disease. *Nature Reviews Neuroscience*, *11*(5), 301.

Mason, S. T., & Fibiger, H. C. (1979). Regional topography within noradrenergic locus coeruleus as revealed by retrograde transport of horseradish peroxidase. *Journal of Comparative Neurology*, *187*(4), 703–724.

Moore, R. Y., & Bloom, F. E. (1979). Central catecholamine neuron systems: Anatomy and physiology of the norepinephrine and epinephrine systems. *Annual Review of Neuroscience*, *2*(1), 113–168.

Nörenberg, W., Schöffel, E., Szabo, B., & Starke, K. (1997). Subtype determination of soma-dendritic α2-autoreceptors in slices of rat locus coeruleus. *Naunyn-Schmiedeberg's Archives of Pharmacology*, *356*(2), 159–165.

Parini, S., Renoldi, G., Battaglia, A., & Invernizzi, R. W. (2005). Chronic reboxetine desensitizes terminal but not somatodendritic α 2-adrenoceptors controlling noradrenaline release in the rat dorsal hippocampus. *Neuropsychopharmacology*, *30*(6), 1048.

Robertson, S. D., Plummer, N. W., De Marchena, J., & Jensen, P. (2013). Developmental origins of central norepinephrine neuron diversity. *Nature Neuroscience*, *16*(8), 1016.

Rodenkirch, C., Liu, Y., Schriver, B. J., & Wang, Q. (2019). Locus coeruleus activation enhances thalamic feature selectivity via norepinephrine regulation of intrathalamic circuit dynamics. *Nature Neuroscience*, *22*(1), 120.

Schwarz, L. A., Miyamichi, K., Gao, X. J., Beier, K. T., Weissbourd, B., DeLoach, K. E., … Luo, L. (2015). Viral-genetic tracing of the input–output organization of a central noradrenaline circuit. *Nature*, *524*(7563), 88.

Seo, D. O., & Bruchas, M. R. (2017). Polymorphic computation in locus coeruleus networks. *Nature Neuroscience*, *20*(11), 1517.

Swanson, L. W. (1976). The locus coeruleus: A cytoarchitectonic, Golgi and immunohistochemical study in the albino rat. *Brain Research*, *110*(1), 39–56.

Takeuchi, T., Duszkiewicz, A. J., Sonneborn, A., Spooner, P. A., Yamasaki, M., Watanabe, M., … Morris, R. G. (2016). Locus coeruleus and dopaminergic consolidation of everyday memory. *Nature*, *537*(7620), 357.

Thiele, A., & Bellgrove, M. A. (2018). Neuromodulation of attention. *Neuron*, *97*(4), 769–785.

Totah, N. K., Neves, R. M., Panzeri, S., Logothetis, N. K., & Eschenko, O. (2018). The locus coeruleus is a complex and differentiated neuromodulatory system. *Neuron*, *99*(5), 1055–1068.

Uematsu, A., Tan, B. Z., Ycu, E. A., Cuevas, J. S., Koivumaa, J., Junyent, F., … Johansen, J. P. (2017). Modular organization of the brainstem noradrenaline system coordinates opposing learning states. *Nature Neuroscience*, *20*(11), 1602.

Wagatsuma, A., Okuyama, T., Sun, C., Smith, L. M., Abe, K., & Tonegawa, S. (2018). Locus coeruleus input to hippocampal CA3 drives single-trial learning of a novel context. *Proceedings of the National Academy of Sciences*, *115*(2), E310–E316.

Williams, J. T., Bobker, D. H., & Harris, G. C. (1991). Synaptic potentials in locus coeruleus neurons in brain slices. *Progress in Brain Research*, *88*, 167–172.

Williams, J. T., North, R. A., Shefner, S. A., Nishi, S., & Egan, T. M. (1984). Membrane properties of rat locus coeruleus neurones. *Neuroscience*, *13*(1), 137–156.

Zhang, Y., Zhang, W., Johnston, A. H., Newman, T. A., Pyykkö, I., & Zou, J. (2010). Improving the visualization of fluorescently tagged nanoparticles and fluorophore-labeled molecular probes by treatment with $CuSO_4$ to quench autofluorescence in the rat inner ear. *Hearing Research*, *269*(1–2), 1–11.

SUPPORTING INFORMATION

Additional supporting information may be found online in the Supporting Information section.

How to cite this article: Wagner-Altendorf TA, Fischer B, Roeper J. Axonal projection-specific differences in somatodendritic α2 autoreceptor function in locus coeruleus neurons. *Eur J Neurosci*. 2019;50:3772–3785. https://doi.org/10.1111/ejn.14553